Journal Name

ARTICLE

Photocatalytic hydrogen evolution driven by platinated CdS nanorods with a hexacyanidoruthenate redox mediator

Hirotsugu Kitano,[a] Atsushi Kobayashi,*[a] Masaki Yoshida[a] and Masako Kato*[a]

Received 00th January 20xx,
Accepted 00th January 20xx

DOI: 10.1039/x0xx00000x

www.rsc.org/

We have investigated the effect of hexacyanidometallate $[M(CN)_6]^{4-}$ (M = Fe, Ru) redox mediators on the photocatalytic H_2 evolution reaction driven by Pt-cocatalyst-loaded cadmium sulfide nanorods (Pt/CdS-NR). A larger amount of H_2 was evolved under blue LED light irradiation ($\lambda = 470 \pm 10$ nm) in the presence of the $[Ru(CN)_6]^{4-}$ than in the presence of $[Fe(CN)_6]^{4-}$, despite the more positive M(III)/M(II) redox potential of $[Ru(CN)_6]^{4-}$ (0.89 V vs NHE) than that of $[Fe(CN)_6]^{4-}$ (0.36 V vs NHE). PXRD and IR spectral experiments during the photocatalytic H_2 evolution reactions clearly indicate that the Prussian white analogue $K_2[CdRu(CN)_6]$ (CdRu-PW) was increasingly formed, producing a white precipitate, whereas only a trace amount of $K_2[CdFe(CN)_6]$ (CdFe-PW) was formed in the reaction with the $[Fe(CN)_6]^{4-}$. The amount of CdRu-PW produced during the photocatalytic H_2 evolution reaction revealed that the electron source of H_2 evolution is gradually changed from the S^{2-} anions generated following the photocorrosion of CdS to the $[Ru(CN)_6]^{4-}$ because of effective hole transfer through the Ru(III)/Ru(II) redox step in the CdRu-PW (1.42 V vs NHE) deposited on the CdS-NR surface. The colourless feature and more positive Ru(III)/Ru(II) redox potential of CdRu-PW than water oxidation suggest that CdRu-PW is a promising hole mediator for solar water splitting.

Introduction

The solar water splitting reaction has attracted considerable attention in recent decades as a promising approach to solve the global energy issue. Since the discovery of the Honda–Fujishima effect,[1] many oxide-based photocatalysts have been developed.[2–6] Although these oxide-based photocatalysts are highly active for the water splitting reaction to produce both H_2 and O_2, most of the oxides only absorb UV light from solar radiation. To extend the absorption band to the visible region, many metal nitrides, oxynitrides, chalcogenides, and oxyhalides have been developed as visible light-driven photocatalysts.[7–26] One typical example of such a photocatalyst is cadmium sulfide (CdS), which has a suitable electronic structure for solar water splitting;[13–18] in particular, CdS can adsorb visible light below 520 nm and its valence band maximum (VBM) and conduction band minimum (CBM) are located at more positive and negative positions than the potentials for water oxidation and reduction reactions, respectively. However, photocorrosion is a crucial issue for most metal chalcogenides, including CdS.[27,28] To suppress photocorrosion, several different types of electron donors (including sacrificial reagents and reversible redox mediators) that effectively receive the hole generated in the metal chalcogenides have been reported.[29] One promising mediator is hexacyanidoferrate, $[Fe(CN)_6]^{4-}$. This mediator can both suppress the photocorrosion of CdS and act as the electron source for the photocatalytic H_2 evolution reaction.[30–35] The key to suppress the photocorrosion was reported to be the *in situ* generation of the Prussian white analogue complex $K_2[CdFe(CN)_6]$ (hereafter CdFe-PW) on the surface of the CdS crystals.[35] The reversible Fe(III)/Fe(II) redox behaviour of CdFe-PW enables it to develop several Z-scheme-type photocatalysts by the combination of an oxide-based O_2 evolving photocatalyst and a CdS-based H_2 evolving photocatalyst to split water to give H_2 and O_2.[36–38] However, the negative redox potential of the Fe(III)/Fe(II) couple (+0.36 V vs NHE) relative to the potential of water oxidation (+0.82 V vs NHE at pH = 7) requires a two-step photoexcitation process to achieve overall water splitting. Given that the VBM of CdS is +1.5 V (vs NHE),[39] the hole transfer from photoexcited CdS* to $[Fe(CN)_6]^{4-}$ consumes approximately half of the absorbed light energy (ca. 2.3 eV).

To overcome this issue, our recent attention has focused on the formation of a Prussian white analogue on the surface of the CdS photocatalyst. Since Prussian white analogues are the one-electron reduced family of Prussian blue complexes, the redox potential of the hexacyanidometalate $[M^{II}(CN)_6]^{4-}$ anion can be widely varied by replacement of the central M^{II} ion.[40–43] In this work, to accept the hole generated in the photoexcited CdS photocatalyst at a more positive potential than $[Fe(CN)_6]^{4-}$, we selected hexacyanidoruthenate, $[Ru(CN)_6]^{4-}$, as the redox mediator to provide the electron to the H_2-evolving CdS photocatalyst, because the Ru(III)/Ru(II) redox potential (+0.89 V vs NHE) is nearly equal to the water oxidation potential at pH = 7. In addition, as expected from the nearly identical molecular

[a] *Department of Chemistry, Faculty of Science, Hokkaido University, North-10 West-8, Kita-ku, Sapporo 060-0810, Japan.*

†Electronic Supplementary Information (ESI) available: TEM, SEM, and EDX spectra of Pt/CdS-NR, results of long-duration photocatalytic H_2 evolution reaction, CV of CdRu-PW-modified ITO electrode, UV-Vis spectra of the reaction solution and *in situ* generated precipitate, and details of estimating the CdRu-PW mass. See DOI: 10.1039/x0xx00000x

structures of $[Ru(CN)_6]^{4-}$ and $[Fe(CN)_6]^{4-}$, several Prussian white analogues have been reported.[44,45] The Pt-cocatalyst-loaded nanorod-shaped CdS (hereafter Pt/CdS-NR) was used as the H_2 evolving photocatalyst because its high photocatalytic performance may enable us to elucidate the replacement effect of the redox mediator from $[Fe(CN)_6]^{4-}$ to $[Ru(CN)_6]^{4-}$.[46–48] Herein, we report the photocatalytic H_2 evolution reaction driven by Pt/CdS-NR in the presence of hexacyanidometalate, $[M(CN)_6]^{4-}$ (M=Fe, Ru) and demonstrate that the *in situ* generated Prussian white analogue $K_2[CdRu(CN)_6]$ (CdRu-PW) acts as a hole mediator at more positive potential than CdFe-PW.

Experimental section

Sample preparation

$CdCl_2 \cdot 2.5H_2O$ and ethylenediamine were purchased from Kanto Chemical Co., Inc. $K_4[Fe(CN)_6] \cdot 3H_2O$ was purchased from Wako Pure Chemical Industries. $K_4[Ru(CN)_6]$ and CdS were purchased from Sigma-Aldrich. Thiourea was purchased from Tokyo Chemical Industry Co., Ltd. Sodium borohydride was purchased from Junsei Chemical Co., Ltd. All reagents and solvents were used without any further purification. If not otherwise specified, all reactions were performed in air. The preparations of nanorod-shaped cadmium sulfide (CdS-NR)[46] and Pt-cocatalyst-loaded Pt/CdS-NR[47] were conducted according to previously published methods.

Preparation of $K_2[CdRu(CN)_6]$ (CdRu-PW). An aqueous solution of $K_4[Ru(CN)_6]$ (20 mM, 10 mL) was added to an aqueous solution of $CdCl_2$ (20 mM, 10 mL) to form white precipitates. After continuous stirring for 1 day at 293 K, the white precipitates were collected by centrifugation and washed several times with methanol. The obtained white powder was dried over silica gel for one night to afford the Prussian white analogue complex $K_2[CdRu(CN)_6]$ as a white powder. Yield: 113 mg (0.197 mmol, 98 %). Anal. Calcd. (%) for $C_6CdK_2N_6Ru \cdot 3.5H_2O$: C, 14.11; H, 1.38; N, 15.31. Found: C, 13.72; H, 1.02; N, 15.72.

Preparation of CdRu-PW-modified ITO electrode. The Prussian white analogue, CdRu-PW-modified ITO electrode was prepared by a slightly modified literature method[40] as follows: A bare ITO electrode was first immersed in a 20 mM $K_4[Ru(CN)_6]$ aqueous solution for 30 min at room temperature and then immersed in a 20 mM $CdCl_2$ aqueous solution for 30 min at room temperature. The obtained $K_2[CdRu(CN)_6]$-modified ITO electrode was washed several times with methanol and then dried over silica gel for one night.

Measurements

UV-vis absorption spectra and diffraction spectra were measured by a Shimadzu UV-2400PC spectrophotometer. The diffraction spectra were transformed using a Kubelka–Munk function, $F(R_\infty)$. IR spectra were measured by a JASCO FT-IR 4100 spectrophotometer using KBr pellets. Powder X-ray diffraction (PXRD) patterns were measured with Cu-K_α (λ= 1.54187 Å) radiation using a Bruker D8 Advance diffractometer equipped with a graphite monochromator and a one-dimensional LinxEye detector. Energy-dispersive X-ray fluorescence (XRF) spectra were recorded on a Bruker S2 PUMA analyzer. Cyclic voltammograms were recorded by a Hokuto Denko HZ-3000 electrochemical measurement system. An acetonitrile solution containing 0.1 M $TBAPF_6$ was used as the electrolyte, and the CdRu-PW-modified ITO electrode, Pt-wire, and Ag/Ag^+ electrodes were used as the working, counter, and reference electrodes, respectively. The sample was degassed with N_2 before the measurements and N_2 was flowed during them. Scanning electron microscopy (SEM) images and energy-dispersive X-ray (EDX) spectra were obtained on a Phenom ProX scanning electron microscope. Transmittance electron microscopy (TEM) images were recorded on a JEOL 2010 FASTEM (200kV).

Photocatalytic H_2 evolution reaction

Under dark conditions, Pt/CdS-NR (2.0 mg) and a small magnetic stirring bar were placed into a hand-made Schlenk flask (volume: 183 mL), and then an acetate buffer solution (5 mL, 200 mM, pH = 5.0) containing $K_4[M(CN)_6]$ (0.01 M; M = Fe or Ru) was added. The sample flask was doubly sealed with rubber septa, and the sample solution was then deoxygenated by Ar bubbling for 1 h. The flask was then irradiated from the bottom with a blue LED light (λ= 470 $\pm$ 10 nm; 20 mW; Opto Device Lab. Ltd., OP6-4710HP2). The temperature was controlled at 298 K using a hand-made aluminium water-cooling jacket with a water-circulating temperature controller (EYELA ACE-1100). Gas samples (0.6 mL) for each analysis were collected from the headspace using a gastight syringe (Valco Instruments Co. Inc.). The amount of evolved H_2 was determined using a gas chromatograph (Agilent 490 Micro Gas Chromatograph).

Results and Discussion

Sample characterization

Figure 1 shows the energy-dispersive XRF spectrum of Pt/CdS-NR to estimate the amount of Pt loaded on CdS-NR. Kα radiation

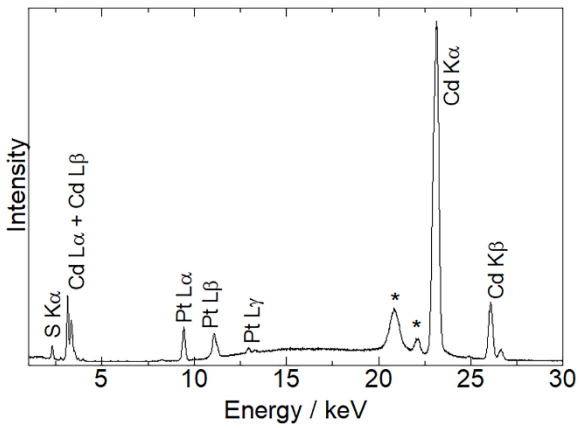

Fig. 1 X-ray fluorescence spectrum of Pt/CdS-NR. Peaks marked by an asterisk originate from the X-ray source as Ag Kα,β radiation.

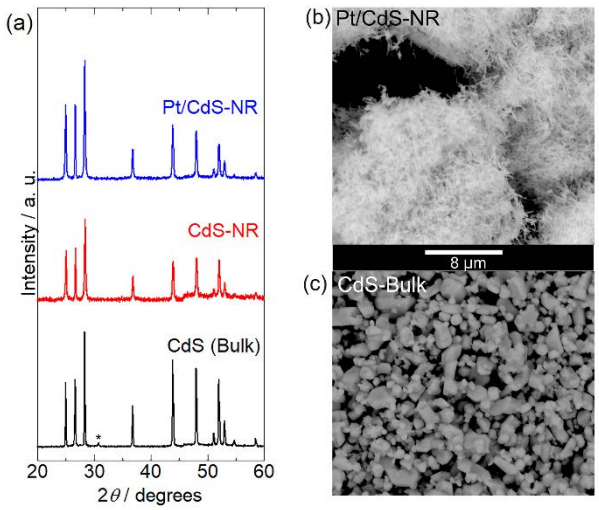

Fig. 2 (a) PXRD patterns of Pt/CdS-NR, CdS-NR samples, and CdS bulk reference. The peak marked by an asterisk of CdS bulk is assigned to CdO on the CdS surface.[49] SEM images of (b) Pt/CdS-NR and (c) CdS bulk. The scale bar (8 μm) is shown between panels (b) and (c).

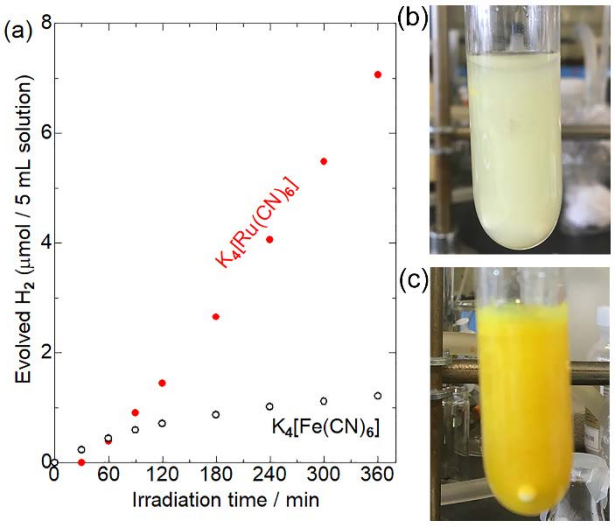

Fig. 3 (a) Photocatalytic hydrogen evolution reaction with Pt/CdS-NR (2.00 mg) in a 200 mM acetate buffer (pH=5.0) that contained 0.01 M $K_4[M(CN)_6]$ as the electron source (black open circles: $K_4[Fe(CN)_6]$; red closed circles: $K_4[Ru(CN)_6]$) under an Ar atmosphere. A blue LED (λ = 470 ± 10 nm) was used as the light source. Photographs of the reaction solutions of (b) $K_4[Ru(CN)_6]$ and (c) $K_4[Fe(CN)_6]$ after light irradiation for 6 h.

derived from S and Cd is clearly observed at approximately 2.38 keV and 23.1 keV, respectively. In addition, Lα and Lβ radiations of Pt are also clearly evident at 9.4 and 11.1 keV, respectively, indicating successful loading of the Pt co-catalyst on the CdS-NR surface. The amount of loaded Pt was estimated to be 0.3 wt%. PXRD patterns and SEM images of Pt/CdS-NR and a bulk sample of CdS are displayed in Figure 2.

Almost an identical PXRD pattern to the bulk CdS, which comprises a wurtzite-type crystal structure, was observed for the synthesized CdS-NR. The PXRD pattern of Pt/CdS-NR was also nearly identical to the other two, suggesting that the crystal structure of CdS-NR hardly changed following deposition of the Pt cocatalyst. Additionally, the (111) and (200) reflections derived from the Pt cocatalyst were scarcely observed, which may be because of its small loading amount and the small size of the Pt nanoparticles. Nevertheless, the TEM image of Pt/CdS-NR clearly indicates that Pt nanoparticles were deposited on the CdS-NR surface (Figure S1). As shown in Figures 2(b) and 2(c), the size of bulk CdS was approximately several μm while the particle size of CdS-NR was estimated to be 50 nm in diameter and 1.0 μm in length, indicating the successful preparation of nanorod-shaped CdS crystals.

Photocatalytic H_2 evolution reaction with $[M(CN)_6]^{4-}$

Figure 3 shows the results of photocatalytic hydrogen evolution reactions using $K_4[M(CN)_6]$ (M = Fe, Ru) as the electron donor. As has been widely reported,[30–35] Pt/CdS-NR evolved ~1.2 μmol of H_2 after light irradiation for 6 h in the presence of $K_4[Fe(CN)_6]$. Slight deactivation of the photocatalytic activity observed after 180 min irradiation might be due to the photoinduced ligand exchange reaction of the one-electron oxidized $[Fe(CN)_6]^{3-}$ anions as suggested by Abe et al.[35] Surprisingly, approximately six-fold more H_2 (7.1 μmol) was evolved in the presence of $K_4[Ru(CN)_6]$ after a 30 min induction period. After irradiation for 24 h, the amount of H_2 evolved in the presence of $[Ru(CN)_6]^{4-}$ was 20.8 μmol (Figure S2). This amount of H_2 is significantly larger than the molar amount of CdS-NR (~14 μmol), suggesting that $[Ru(CN)_6]^{4-}$ serves as an electron donor for the H_2 evolution reaction, even if electron-donating S^{2-} anions were generated by the photocorrosion of CdS-NR. Notably, a larger amount of H_2 was evolved in the presence of $[Ru(CN)_6]^{4-}$ than that in $[Fe(CN)_6]^{4-}$ despite the more positive M(III)/M(II) redox potential of $[Ru(CN)_6]^{4-}$ (+0.89 V vs NHE) than that of $[Fe(CN)_6]^{4-}$ (+0.36 V vs NHE). Note that negligible amount of H_2 was generated in the absence of $[M(CN)_6]^{4-}$ (M = Fe, Ru) in acetate buffer solution (Figure S3), indicating that the acetate anion did not act as the electron source for H_2 evolution reaction.

To elucidate the differences between these two $[M(CN)_6]^{4-}$, we first examined their adsorption behaviours on the CdS-NR surface based on their zeta potentials. The zeta potentials in aqueous solutions of $[Fe(CN)_6]^{4-}$ and $[Ru(CN)_6]^{4-}$ were comparable at approximately −30 mV, which was significantly shifted to the negative than it is in the absence of the $[M(CN)_6]^{4-}$ (Table S1). Thus, as expected from their similar molecular structures, the CdS-NR surface was negatively charged following adsorption of $[M(CN)_6]^{4-}$ anions, and the difference in the extent of adsorption between these two $[M(CN)_6]^{4-}$ should be negligible. However, a large colour difference of the dispersed solutions is observed after a 6 h photocatalytic H_2 evolution reaction; a large amount of white precipitate formed in the reaction solution with the $[Ru(CN)_6]^{4-}$ while only a yellow suspension of Pt/CdS-NR was observed for the solution with $[Fe(CN)_6]^{4-}$ as shown in Figures 3(b) and 3(c).

To identify the white precipitate formed in the reaction solution with $[Ru(CN)_6]^{4-}$, PXRD and IR spectral measurements of the precipitates isolated from the reaction solution by centrifugation were conducted. Figure 4(a) shows the IR spectra

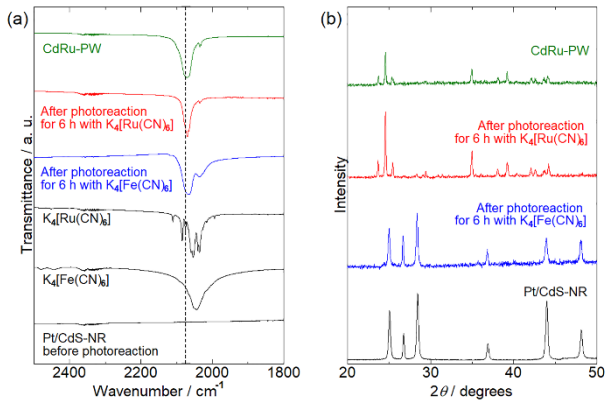

Fig. 4 (a) IR spectra of Pt/CdS-NR before and after photocatalytic H_2 evolution reactions in comparison with the spectra of $K_4[M(CN)_6]$ (M= Fe, Ru) mediators and the Prussian-white analogue CdRu-PW. Dotted line indicates the peak position of ν(C≡N) mode of CdRu-PW. (b) PXRD patterns of the Pt/CdS-NR before and after photocatalytic H_2 evolution reactions for 6 h in comparison with the pattern of CdRu-PW.

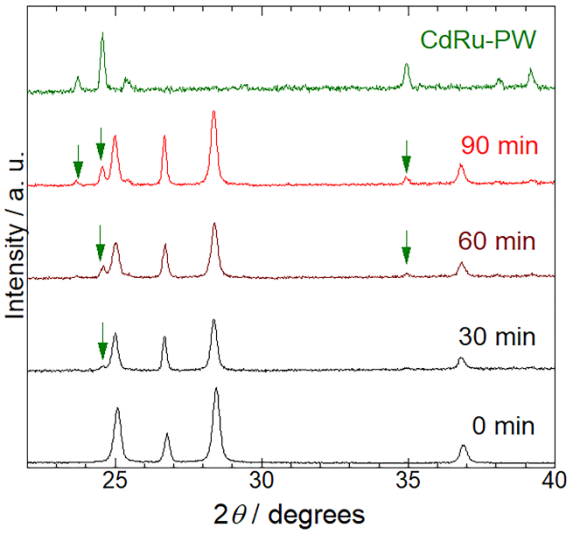

Fig. 5 Changes of the PXRD pattern of Pt/CdS-NR in the photocatalytic H_2 evolution reaction with $K_4[Ru(CN)_6]$ redox mediator. The top green line shows the pattern of Prussian-white analogue CdRu-PW. Green arrows indicate the diffraction peaks derived from CdRu-PW.

of the precipitates. As reported in the literature, $K_4[Fe(CN)_6]$ and $K_4[Ru(CN)_6]$ exhibit stretching vibrations of the cyanido ligand ν(C≡N) at 2043 cm^{-1} and 2054 cm^{-1}, respectively. Although no peak was observed in this region for Pt/CdS-NR prior to the photocatalytic H_2 evolution reaction, a peak similar to that observed for $K_4[M(CN)_6]$ was observed for the precipitates isolated from the reaction solution with $K_4[M(CN)_6]$ (M = Fe, Ru) after 6 h of light irradiation. Notably, the peak position attributable to the ν(C≡N) mode shifted to higher wavelength (by approximately 20 cm^{-1}) relative to that of $K_4[M(CN)_6]$. It was previously reported that the Prussian white analogue $K_2[CdFe(CN)_6]$ (hereafter CdFe-PW) was *in situ* generated on the CdS surface in the photocatalytic H_2 evolution reaction in the presence of the $[Fe(CN)_6]^{4-}$ because of the partial photocorrosion of CdS, which provides Cd^{2+} ions to form CdFe-PW.[35] The peak position of the ν(C≡N) mode is known to shift to higher wavelength by bridging two metal centers.[50] Thus, the higher-wavelength-shifted ν(C≡N) vibrations observed for the precipitates clearly suggest the *in situ* formation of Prussian white analogues (CdFe-PW or CdRu-PW) during the photocatalytic H_2 evolution reaction. In fact, the Prussian white analogue CdRu-PW prepared by a simple solution reaction (see Preparation of $K_2[CdRu(CN)_6]$) exhibited a ν(C≡N) vibration at almost an identical position (2072 cm^{-1}) to that observed for the precipitates.

Figure 4(b) shows the PXRD patterns of the precipitates isolated from the reaction solutions after 6 h irradiation. The PXRD pattern of the precipitate obtained from the reaction solution with $K_4[Fe(CN)_6]$ was almost identical to that of the original Pt/CdS-NR. In contrast, the pattern for the precipitate isolated from the reaction solution with $K_4[Ru(CN)_6]$ was completely different to the original Pt/CdS-NR and qualitatively agreed with that of CdRu-PW. These contrasting results clearly indicate a significant difference in production of the Prussian white complexes involving these two $[M(CN)_6]^{4-}$; a relatively large amount of CdRu-PW was produced as the by-product during the photocatalytic H_2 evolution reaction while only a trace amount of CdFe-PW was produced on the CdS-NR surface.

In fact, many block-shaped microcrystals were observed for the precipitate in the SEM image, and X-ray fluorescence derived from K, Cd, and Ru were clearly observed in the EDX spectra (Figures S4 and S5). Further, the number of block-shaped microcrystal of CdRu-PW observed in in SEM image and the peak intensities of the Ru Lα and Lβ radiations in EDX spectra were increased by increasing the light irradiation time.

To characterize the production mechanism of CdRu-PW during the photocatalytic hydrogen evolution reaction in the presence of $K_4[Ru(CN)_6]$, PXRD analysis was conducted for the samples isolated at 30 min irradiation intervals. As shown in Figure 5, diffraction peaks originating from Pt/CdS-NR were observed for all the samples used in these measurements. Notably, diffraction peaks assignable to CdRu-PW (indicated by green arrows in Figure 5) gradually appeared as the irradiation time increased, indicating growth of CdRu-PW microcrystals during the photocatalytic H_2 evolution reaction. Actually, the SEM images of these samples clearly indicate that the number of block crystals of CdRu-PW increased by increasing the light irradiation time (Figures S4(a) to S4(e)). It should be noted that the induction period (~30 min) in the photocatalytic H_2 evolution reaction in the presence of the $K_4[Ru(CN)_6]$ almost corresponds with the time for the production of CdRu-PW, and the amount of CdRu-PW produced seems to increase as the irradiation time is increased. Because elucidating the actual electron source for H_2 evolution under these conditions is crucial, we examined the change of the sample mass after photocatalytic H_2 evolution by isolating the insoluble precipitates via centrifugation to estimate the amount of CdRu-PW produced, as Cd^{2+} cations generated from the photocorrosion of CdS-NR are necessary to produce CdRu-PW. Our preliminary experiments based on UV-Vis spectroscopy roughly estimated the solubility product of CdFe-PW and CdRu-

PW (K_{SP} = 7.8 × 10^{-10} and 1.7 × 10^{-12} ($mol^2 \cdot L^{-2}$), respectively) to be comparable to the widely known insoluble AgCl (1.7 × 10^{-10} $mol^2 \cdot L^{-2}$), suggesting that dissolution of these Prussian white analogues to water was negligible in these experiments. The original sample mass before the photocatalytic H_2 evolution reaction was 2.00 mg (corresponding to the mass of Pt/CdS-NR only), because the $K_4[Ru(CN)_6]$ mediator was completely dissolved in the acetate buffer solution. Interestingly, the sample masses in the presence of $K_4[Ru(CN)_6]$ after 6 and 21 h of irradiation increased to 3.98 and 4.50 mg, respectively, suggesting the production of CdRu-PW. These values are significantly larger than that after 6 h of irradiation in the $K_4[Fe(CN)_6]$ solution (2.52 mg). In the photocorrosion process of CdS-NR, not only Cd^{2+} cations but also the same molar amount of S^{2-} anions would be produced. The S^{2-} anion is a well-known sacrificial donor to donate two electrons to form H_2,[46–48] and the potential for the photocorrosion CdS to donate two electrons was reported to be 0.32 V vs NHE.[51] Thus, to estimate the amount of CdRu-PW produced, we assumed that the following photochemical reaction occurs:

$$CdS + aK_4[Ru(CN)_6] + 2aH^+ \rightarrow$$
$$(1-a)\ CdS + a\{K_2[CdRu(CN)_6]\} + 2aK^+ + aS + aH_2 \quad (1)$$

where *a* denotes the molar ratio of photocorroded CdS-NR and the same molar amounts of CdRu-PW, S^0, and H_2 are assumed to be generated. Note that the $[Ru(CN)_6]^{4-}$ in this scenario does not transfer any electrons to the Pt/CdS-NR photocatalyst to generate H_2 and the electron source of evolved H_2 is S^{2-}, which originates from the photocorrosion of CdS-NR. Table 1 summarizes the estimated amount of CdRu-PW produced based on Eq. (1) and compares the amount of H_2 generated. Details of the calculations are given in the Electronic Supplementary Information ("Estimation of the amount of CdRu-PW produced"). After 6 h of light irradiation, ~43% of CdS-NR was estimated to be photocorroded to produce 5.9 μmol of CdRu-PW; the same molar amount of S^{2-} should be generated to act as the sacrificial electron donor. However, GC analysis clearly shows that more H_2 (~7.5 μmol) was evolved than S^{2-} was consumed after 6 h of irradiation (Figure 3(a)). Given that a negligible amount of H_2 was evolved when the insoluble CdRu-PW was used as the electron source instead of $K_4[Ru(CN)_6]$ (Figure S3), this result clearly indicates the contribution of the $[Ru(CN)_6]^{4-}$ as an electron source for H_2 evolution; that is, at least 3.2 μmol of the $[Ru(CN)_6]^{4-}$ would donate one electron to the Pt/CdS-NR photocatalyst to produce 1.6 μmol of H_2 (corresponding to the difference between the molar amounts of evolved H_2 and produced CdRu-PW). In other words, ~21% of the electrons to form 7.5 μmol of H_2 would originate from the $[Ru(CN)_6]^{4-}$. Notably, the amount of H_2 evolved after 21 h of irradiation increased to 20.8 μmol on the basis of GC analysis, whereas the amount of CdRu-PW produced, as estimated from the measured sample mass and Eq. (1), was only ~7.5 μmol. This estimation clearly indicates that over 60% of the electrons required to evolve 20.8 μmol of H_2 should be derived from the $[Ru(CN)_6]^{4-}$. Thus, the contribution of $[Ru(CN)_6]^{4-}$ to the photocatalytic H_2 evolution reaction as an electron source

Table 1. Change of the insoluble sample mass in the photocatalytic H_2 evolution reaction.

Redox mediator	Irradiation time (h)	Sample mass (mg)	Photo-corroded CdS-NR (mol%)[a]	CdM-PW produced (μmol)[a]	H_2 evolved (μmol)[b]
$[Ru(CN)_6]^{4-}$	0	2.00	0	-	-
$[Ru(CN)_6]^{4-}$	6	3.98	42.8	5.92	7.5
$[Ru(CN)_6]^{4-}$	21	4.50	54.1	7.47	20.8
$[Fe(CN)_6]^{4-}$	6	2.52	12.0	1.11	1.2

[a] Estimated by Eq. (1). [b] Estimated by GC analysis.

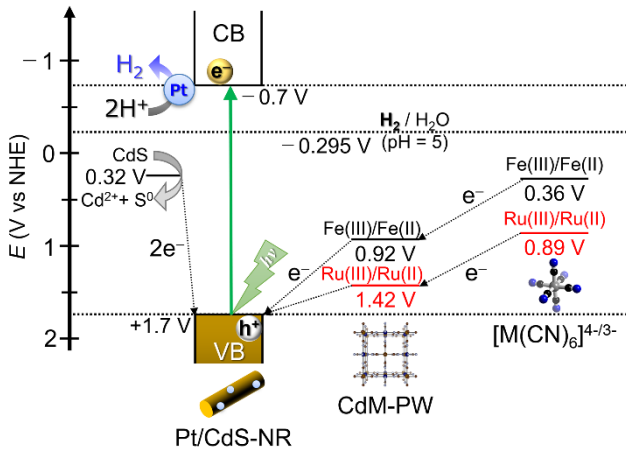

Scheme 1 Schematic energy diagram for the photocatalytic H_2 evolution reaction driven by Pt/CdS-NR in the presence of $K_4[M(CN)_6]$ (M = Fe, Ru) redox mediators.

increased significantly as the irradiation time increased. Considering that a large amount of CdRu-PW was simultaneously generated during this reaction, one plausible mechanism for the increasing contribution of $[Ru(CN)_6]^{4-}$ is that the *in situ* generated CdRu-PW may act as a hole mediator/accumulator to transfer the hole generated in Pt/CdS-NR to the $[Ru(CN)_6]^{4-}$ species in solution. In fact, CV measurements for the CdRu-PW-modified ITO electrode clearly reveal that CdRu-PW exhibits a quasi-reversible Ru(III)/Ru(II) redox wave at 1.42 V (vs NHE, Figure S6), which is just above the valence band maximum of CdS-NR (~1.7 V vs NHE)[39] and more positive than the Ru(III)/Ru(II) redox couple of $[Ru(CN)_6]^{4-}$ in aqueous solution (0.89 vs NHE).

Mechanistic aspects of photocatalytic H_2 evolution with $[M(CN)_6]^{4-}$

As discussed in the "Photocatalytic H_2 evolution reaction with $[M(CN)_6]^{4-}$" section, replacement of the electron mediator from the widely used $[Fe(CN)_6]^{4-}$ to its Ru(II) analogue $[Ru(CN)_6]^{4-}$ greatly affects the photocatalytic H_2 evolution reaction. In this section, we discuss the mechanistic differences of this reaction for these two hexacyanidometallates. Scheme 1 shows a schematic energy diagram for the photocatalytic H_2 evolution reaction using a Pt/CdS-NR photocatalyst and a $K_4[M(CN)_6]$ (M = Fe, Ru) mediator. In the reaction with the $[Fe(CN)_6]^{4-}$, as reported previously,[35] a trace amount of CdFe-PW is initially generated on the Pt/CdS-NR surface and functions as an effective mediator to transfer the hole from CdS-NR to $[Fe(CN)_6]^{4-}$. This is supported by the results showing a small

change of the sample mass after the reaction (~0.5 mg) and the formation of one-electron oxidized $[Fe^{III}(CN)_6]^{3-}$ in the UV-Vis spectrum (Figure S7). By comparison, in the reaction with $[Ru(CN)_6]^{4-}$, the M(III)/M(II) redox potential of $[Ru(CN)_6]^{4-}$ is more positive than that of $[Fe(CN)_6]^{4-}$ (Scheme 1). In this case, the one-electron oxidized $[Ru(CN)_6]^{3-}$ species generated by accepting the hole from the photoexcited Pt/CdS-NR rapidly recombines with the excited electron to revert to its initial state, or it oxidizes the S^{2-} anion on the CdS-NR surface to generate Cd^{2+} cations. Given that a two-electron oxidation is required for the conversion of S^{2-} to S^0, the observed induction period of ~30 min would be caused by the recombination process between the one-electron oxidized $[Ru^{III}(CN)_6]^{3-}$ species and the excited electron in Pt/CdS-NR. As a result, the photocatalytic H_2 evolution reaction in the initial several hours is mainly driven by the consumption of S^{2-} anions as the electron source, with a large amount of CdRu-PW (~5.9 μmol) produced as the by-product of photocorrosion. This photocorrosion process was observed as a decrease of the band-gap transition intensity in the UV-Vis diffuse reflectance spectra of the Pt/CdS-NR isolated by centrifugation from the reaction solution (Figure S8). As the CdS-NR surface becomes covered by CdRu-PW, however, the electron source for H_2 evolution is replaced from S^{2-} to $[Ru(CN)_6]^{4-}$, because the CdRu-PW deposited on the CdS-NR surface not only suppresses the photocorrosion of CdS-NR as a surface passivating layer but also improves the hole transfer efficiency from the photoexcited CdS-NR to the $[Ru(CN)_6]^{4-}$ in solution by its reversible Ru(III)/Ru(II) redox mediating/accumulating ability. Unfortunately, however, the surface passivating effect by the *in situ* generated CdRu-PW in our present reaction is not sufficient to suppress the photocorrosion of CdS-NR, resulting in the photocorrosion of over 50% of CdS-NR after 21 h of irradiation even in the presence of the 3-times higher concentration of $K_2[Ru(CN)_6]$ (see Figure S9).

Conclusions

In this work, we have investigated the photocatalytic H_2 evolution reaction driven by Pt-co-catalyst loaded nanorod-shaped CdS (Pt/CdS-NR) by using two different redox mediators, the widely used hexacyanidoferrate $[Fe(CN)_6]^{4-}$ and its Ru(II) analogue $[Ru(CN)_6]^{4-}$. Interestingly, more H_2 was evolved in the presence of $[Ru(CN)_6]^{4-}$ than in the presence of $[Fe(CN)_6]^{4-}$ despite the more positive Ru(III)/Ru(II) redox potential than that of the Fe(III)/Fe(II) couple. PXRD and IR spectral experiments clearly indicate that only a trace amount of CdFe-PW was formed on the surface of Pt/CdS-NR in the photocatalytic H_2 evolution reaction in the presence of $[Fe(CN)_6]^{4-}$, whereas the Ru(II) analogue CdRu-PW was increasingly formed when a $K_4[Ru(CN)_6]$ aqueous solution was used as the electron source. Our careful analysis on the amount of CdRu-PW produced during the photocatalytic H_2 evolution reaction suggests that the electron source for H_2 evolution was gradually changed from S^{2-} anions generated by the photocorrosion of CdS-NR to the $[Ru(CN)_6]^{4-}$, due to the hole mediating ability of the CdRu-PW deposited on the CdS-NR surface. Since the CdRu-PW is colourless and the Ru(III)/Ru(II) redox potential is more positive than the potential of water oxidation, it could be a promising hole mediating material for solar water splitting that would not suppress the light absorption of photocatalyst/photosensitizer. Further studies to suppress the photocorrosion of CdS-NR viz. formation of a thin film composed of Prussian white analogues is now progress.

Conflicts of interest

There are no conflicts to declare.

Acknowledgements

The authors thank Dr. Y. Shibata (Bruker, Japan) for the valuable support with the XRF measurements. This study was supported by the Shimadzu Science Foundation, Shorai Science and Technology Foundation, Murata Science Foundation, Grants-in-Aid for Scientific Research (C)(26410063), Artificial Photosynthesis (area No. 2406, No.15H00858), and Soft Crystals (area No. 2903, No. JP17H06367) from MEXT, Japan.

References

1 A. Fujishima and K. Honda, *Nature* 1972, **238**, 37–38.
2 M. D. Hernandez-Alonso, F. Fresno, S. Suareza and J. M. Coronado, *Energy Environ. Sci.*, 2009, **2**, 1231–1257.
3 A. Kudo and Y. Miseki, *Chem. Soc. Rev.*, 2009, **38**, 253–278.
4 X. Chem, S. Shen, L. Guo and S. S. Mao, *Chem. Rev.*, 2010, **110**, 6503–6570.
5 K. Maeda, *ACS Catal.* 2013, **3**, 1486–1503.
6 J. Yang, D. Wang, H. Han and C. Li, *Acc. Chem. Res.*, 2013, **46**, 1900–1909.
7 K. Maeda, T. Takata, M. Hara, N. Saito, Y. Inoue, H. Kobayashi and K. Domen, *J. Am. Chem. Soc.*, 2005, **127**, 8286–8287.
8 Y. Lee, H. Terashima, Y. Shimodaira, K. Teramura, M. Hara, H. Kobayashi, K. Domen and M. Yashima, *J. Phys. Chem. C*, 2007, **111**, 1042–1048.
9 K. Maeda, M. Higashi, D. Lu, R. Abe and K. Domen, *J. Am. Chem. Soc.*, 2010, **132**, 5858–5868.
10 R. Abe, M. Higashi and K. Domen, *J. Am. Chem. Soc.*, 2010, **132**, 11828–11829.
11 K. Maeda, M. Higashi, B. Siritanaratkul, R. Abe and K. Domen, *J. Am. Chem. Soc.*, 2011, **133**, 12334–12337.
12 C. Pan, T. Takata, M. Nakabayashi, T. Matsumoto, N. Shibata, Y. Ikuhara and K. Domen, *Angew. Chem. Int. Ed.*, 2015, **54**, 2955–2959.
13 Y. Nosaka, K. Yamaguchi, A. Kuwabara, H. Miyama. R. Baba and A. Fujishima, *J. Photochem. Photobiol. A*, 1992, **64**, 375–382.
14 J.-F. Reber and M. Rusek, *J. Phys. Chem.*, 1986, **90**, 824–834.
15 D. Jing and L. Guo, *J. Phys. Chem. B*, 2006, **110**, 11139–11145.
16 X. Zong, H. Yan, G. Wu, G. Ma, F. Wen, L. Wang and C. Li, *J. Am. Chem. Soc*. 2008, **130**, 7176–7177.
17 N. Bao, L. Shen, T. Takata and K. Domen, *Chem. Mater.*, 2008, **20**, 110–117.
18 H. Yan, J. Yang, G. Ma, G. Wu, X. Zong, Z. Lei, J. Shi and C. Li, *J. Catalysis*, 2009, **266**, 165–168.
19 C. Xing, Y. Zhang, W. Yan and L. Guo, *Int. J. Hydrogen Energy*, 2006, **31**, 2018–2024.
20 X. Wang, G. Liu, Z.-G. Chen, F. Li, L. Wang, G. Q. Lu and H.-M. Cheng, *Chem. Commun.*, 2009, **23**, 3452–3454.

21 Q. Li, B. Guo, J. Yu, J. Ran, B. Zhang, H. Yan and J. R. Gong, *J. Am. Chem. Soc.*, 2011, **133**, 10878–10884.
22 J. Zhang, J. Yu, M. Jaroniec and J. R. Gong, *Nano Lett.*, 2012, **12**, 4584–4589.
23 Z. Han, F. Qiu, R. Eisenberg, P. L. Holland and T. D. Krauss, *Science*, 2012, **338**, 1321–1324.
24 K. Sawaguchi-Sato, A. Kobayashi, M. Yoshida and M. Kato, *J. Photochem. Photobiol. A*, 2017, **335**, 182–189.
25 H. Kunioku, M. Higashi, O. Tomita, M. Yabuuchi, D. Kato, H. Fujito, H. Kageyama and R. Abe, *J. Mat. Chem. A*, 2018, **6**, 3100–3107.
26 H. Kunioku, A. Nakada, M. Higashi, O. Tomita, H. Kageyama and R. Abe, *Sustainable Energy Fuels*, 2018, in press. (DOI: 10.1039/c8se00097b)
27 R. Williams, *J. Chem. Phys.*, 1960, **32**, 1505–1507.
28 D. J. Fermín, E. A. Ponomarev and L. M. Peter, *J. Electroanal. Chem.*, 1999, **473**, 192–203.
29 T. Inoue, T. Watanabe, A. Fujishima, K. Honda and K. Kohayakawa, *J. Electrochem. Soc.*, 1977, **124**, 719–722.
30 H.-D. Rubin, B. D. Humphrey and A. B. Bocarsly, *Nature*, 1984, **308**, 339
31 H.-D. Rubin, D. J. Arent, B. D. Humphrey and A. B. Bocarsly, *J. Electrochem. Soc.*, 1987, **134**, 93–101.
32 Y. Tachibana, K. Umekita, Y. Otsuka and S. Kuwabata, *J. Phys. D: Appl. Phys.*, 2008, **41**, 102002.
33 R. M. Evangelista, S. Makuta, S. Yonezu, J. Andrews and Y. Tachibana, *ACS Appl. Mater. Interfaces*, 2016, **8**, 13957–13965.
34 Z. Li, W. Wang, C. Ding, Z. Wang, S. Liao and C. Li, *Energy Environ. Sci.*, 2017, **10**, 765–771.
35 T. Shirakawa, M. Higashi, O. Tomita and R. Abe, *Sustainable Energy Fuels*, 2017, **1**, 1065–1073.
36 W. Wang, J. Chen, C. Li and W. Tian, *Nat. Commun.*, 2014, **5**, 4647.
37 L. J. Zhang, S. Li, B. K. Liu, D. J. Wang and T. F. Xie, *ACS Catal.*, 2014, **4**, 3724–3734.
38 T. Kato, Y. Hakari, S. Ikeda, Q. Jia, A. Iwase and A. Kudo, *J. Phys. Chem. Lett.*, 2015, **6**, 1042–1047.
39 L. E. Brus, *J. Chem. Phys.*, 1984, **80**, 4403–4409.
40 K. Itaya, T. Ataka and S. Toshima, *J. Am. Chem. Soc.*, 1982, **104**, 4767–4772.
41 K. Itaya, I. Uchida and V. D. Neff, *Acc. Chem. Res.*, 1986, **19**, 162–168.
42 F. Scholz and A. Dostal, *Angew. Chem. Int. Ed.*, 1995, **34**, 2685–2687.
43 A. A. Karyakin, *Electroanalysis*, 2001, **13**, 813–819.
44 J. N. Behera, D. M. D'Alessandro, N. Soheilnia and J. R. Long, *Chem. Mater.*, 2009, **21**, 1922–1926.
45 E. Reguera, A. Gomez, J. Balmaseda, G. Contreras and A. Escamilla, *Stru. Chem.*, 2001, **12**, 59–66.
46 J. S. Jang, U. A. Joshi and J. S. Lee, *J. Phys. Chem. C*, 2007, **111**, 13280–13287.
47 J. Jin, J. Yu, G. Liu and K. Wong, *J. Mater. Chem. A.*, 2013, **1**, 10927–10934.
48 Z. Sun, H. Zheng, J. Li and P. Du, *Energy Environ. Sci.*, 2015, **8**, 2668–2677.
49 Y. Fan, M. Deng, G. Chen, Q. Zhang, Y. Luo, D. Li and Q. Meng, *J. Alloys Compd*. 2011, **509**, 1477–1481.
50 K. Nakamoto, Infrared and Raman Spectra of Inorganic and Coordination Compounds, Part B, Sixth Edition, p110–117, Wiley, **2008**.
51 A. J. Bard, M. S. Wrighton, *J. Electrochem. Soc.*, 1977, **124**, 1706–1710.